Petroleum Science 20 (2023) 776–786

Contents lists available at ScienceDirect

Petroleum Science

journal homepage: www.keaipublishing.com/en/journals/petroleum-science

Original Paper

Effects of deep alkaline and acidic fluids on reservoir developed in fault belt of saline lacustrine basin

Lei-Lei Yang [a, b], Xin-Wei Li [a, b], Guo Wei [a, b], Yi-Dan Liu [c], Qin-Gong Zhuo [d], Zhi-Chao Yu [d], Zhi-Ye Gao [a, b, *]

[a] State Key Laboratory of Petroleum Resource and Prospecting, China University of Petroleum (Beijing), Beijing, 102249, China
[b] The Unconventional Petroleum Research Institute, China University of Petroleum (Beijing), Beijing, 102249, China
[c] Jilin Oilfield Company, Jilin, 130062, China
[d] PetroChina Exploration and Development Research Institute, Beijing, 100083, China

ARTICLE INFO

Article history:
Received 30 August 2021
Received in revised form
15 April 2022
Accepted 18 September 2022
Available online 22 September 2022

Edited by Jia-Jia Fei

Keywords:
Saline lacustrine basin
Alkaline and acidic fluids
Fault-belt reservoir
Mineral transformation
Physical conditions

ABSTRACT

Through the long development processes of reservoir sedimentation and diagenesis, acidic and alkaline fluids play key roles in controlling deep reservoir development. However, the ways in which deep fluids control and transform the reservoir under complex fault conditions remain unclear. In this study, a 2D model was established based on a typical sub-salt to intra-salt vertical profile in the Qaidam Basin, China. Based on measured data, multiphase flow reaction and solute transport simulation technology were used to analyze fluids flow and migration in the intra-salt and sub-salt reservoirs, determine the mineral dissolution, precipitation, and transformation in the reservoir caused by the deep fluids, and calculate the changes in reservoir porosity. Results show that deep fluid migrates preferentially along dominant channels and triggers a series of fluid–rock chemical reactions. In the first stage, a large amount of anhydrite precipitated in the fault as a result of upward migration of deep saline fluid, resulting in the formation of anhydrite veins and blockage at the base of the fault. In the second stage, organic acids caused minerals dissolution and a vertical channel was opened in previously blocked area, which promoted continuous upward migration of organic acids and the formation of secondary pores. This study clarifies the transformative effects of deep alkaline and acidic fluids on the reservoir. Moreover, the important fluid transport role of faults and their effect on reservoir development were determined.

1. Introduction

Important oil/gas exploration breakthroughs have been made consecutively in saline lacustrine basins, and understanding their development process is indispensable (Williams et al., 2014; Rosenberg et al., 2015; Warren, 2016; Wu et al., 2019; Zou et al., 2019). In saline lacustrine basin, the overpressure zone and various salt structures often form beneath gypsum layer, which affects the reservoir development and provides space and channels for the oil/gas accumulation and migration (Jackson and Hudec, 2017; King and Morley, 2017; Gaël et al., 2018). The deep fluids in the oil/gas-rich basin is diverse and complex. Through flow and migration via dominant channels, a series of constructive or destructive transformations of the reservoir caused by deep fluids occurs. At present, the control effect of deep fluids on abnormal high-pressure fault zone reservoirs remains unclear, which leads to incomplete understanding of the development mechanisms of the oil/gas reservoirs and restricts exploration and development of oil/gas resources.

The Qaidam Basin has been under the effects of uplift of the Qinghai–Tibet Plateau since the Cenozoic. The continuous phased uplift has resulted in elevation of the basin, closure of the lake basin, a dry and cold climate, and a sufficient source of salt, thus forming a typical plateau saline lake basin (Huang et al., 2016; Zhang et al., 2017a). The unique mixed sedimentary environment of the plateau saline lake basin leads to thinner sand bodies and generally developed cementation, so the connectivity of sand bodies is poor. The 'self-closed' formation fluid causes the key aspect of formation of reservoirs to be the transport capacity of the

* Corresponding author. State Key Laboratory of Petroleum Resource and Prospecting, China University of Petroleum (Beijing), Beijing, 102249, China.
E-mail address: gaozhiye@cup.edu.cn (Z.-Y. Gao).

https://doi.org/10.1016/j.petsci.2022.09.020

fault–sand body transport system (Yoseph and Warren, 2002; David et al., 2014). Faults provide preferential channels for fluids and play an important role in the development of such reservoirs (Chiaramonte et al., 2011; Watanabe et al., 2013; Huang et al., 2016).

In the Oligocene E_3^2 reservoir in the Yingxi area of the Qaidam Basin, salt ions mainly enter the reservoir with deep fluids via faults, which has a significant impact on the reservoir. From isotopic and other studies, many scholars have concluded that the Quaternary sediments in the Qaidam Basin have essentially no seawater supply and that the main source of lake water ions is deep circulating water (Chen and Ren, 2019; Shi et al., 2019; Hao et al., 2020). Other scholars have shown that the gypsum rock in the Shizigou area of the Qaidam Basin is salt-forming in the deep fluid (Jian et al., 2014). In the Oligocene period, affected by the strike-slip nappe movement of the Eastern Kunlun Orogenic Belt, fault formation became strong, providing good channels for deep hydrothermal upwelling (Zhang et al., 2016; Hao et al., 2020). As a result of expansion under the high temperature and the compression, deep brine upwelled along the faults, along with the adjacent formation fluid, thus forming a deep hot-brine cycle (Sisavath et al., 2012; Han et al., 2019). Moreover, co-deposition of zeolite and iron-bearing dolomite occurred in the gypsum–salt strata in this area. The co-deposition of analcite and iron-bearing dolomite is considered a result of hydrothermal exhalative sedimentation at the bottom of the lake basin (Pham et al., 2012; Simpson and Bignall, 2016).

Fluid-rock chemical reaction extends through the entire diagenetic process, particularly when acidic fluid is involved (Belén et al., 2011; Németh et al., 2015; Hélène et al., 2020). The interaction between acidic fluid and rock under high-temperature and high-pressure formation conditions leads to dissolution, cementation, and transformation of minerals, which are main determining factors of reservoir porosity. Organic acids are quite common in the reservoir development process of oil/gas basins. In addition to being generated directly through the thermal evolution process of source rocks, organic acids can also be generated by thermal chemical-reduction reactions involving hydrocarbons and sulfates in late-stage diagenesis. These processes provide an acidic environment for the formation system (Frolov et al., 2016; Covas et al., 2019). Anhydrite is widely distributed in the study area within a saline lake basin sedimentary environment. Under the acidic, high-temperature, and high-pressure environment, anhydrite has an important influence on the development of dissolution porosity or the precipitation of calcite (Acero et al., 2015). Dissolution of anhydrite increases the porosity and permeability of the rocks, thus improving pore structure. Conversely, anhydrite dissolution releases abundant calcium ions, prompting calcite precipitation and diminishing reservoir space. In general, the reduction of reservoir space caused by calcite precipitation is less than the increase in reservoir space caused by the dissolution of soluble minerals, such as anhydrite and feldspar. Thus, the effects of acidic fluid provide a certain enhancement of reservoir physical properties (Austad et al., 2010; Wilke et al., 2012; Seyyedi et al., 2020).

In this study, the typical geological profile of the Yingxi area in the Qaidam Basin was selected to establish a 2D profile model. The fluid–rock chemical reactions caused by deep saltwater and organic acid-rich fluids entering the reservoir were simulated. The laws of mineral dissolution, precipitation, and transformation were analyzed, and the transformation of reservoir porosity was calculated to determine whether the deep fluid led to a large amount of salt mineral precipitation, and thus to reservoir obstruction, and whether the incursion of organic acid-rich fluids in the late stage could improve the physical properties of the reservoir. Thus, the goal of the study was to determine the transformation effect of the deep saltwater and the organic acid-rich fluid on the reservoir under the condition of its fault structure. The results are helpful to reveal the controlling effect of deep fluid on reservoir, especially the reservoir developed in fault belt. Furthermore, the development mechanism of reservoirs in saline lacustrine basin could be determined to improve exploration efficiency.

2. Geological background

The Qaidam Basin is a Mesozoic, continental, hydrocarbon-bearing basin within the Altun, Kunlun, and Qilian Mountains, as shown in Fig. 1a and b (Liu et al., 2017; Zhang et al., 2017b; Shi et al., 2019). Under the dynamic background of India–Eurasia plate collision, left-lateral strike-slip motion of the Altun Fault occurred in the Eocene and gradually migrated to the Qaidam Basin to the northeast, resulting in thrust-nappe and strike-slip deformation along NW–SE trending faults at the northern margin of the Qaidam–Qilianshan area (Guo et al., 2017; Hao et al., 2020). Therefore, the western Qaidam area is characterized by a sagging sedimentary region under the extensional tectonic background (Wang et al., 2020).

The Yingxi area was in the center area of lacustrine deposition during the Oligocene, and lake carbonate was the most important type of rock that developed (Ma et al., 2019; Shi et al., 2020). It has a mixed origin, containing clastic particles, argillaceous components, and salt minerals. The reservoir profile in the western Qaidam Basin is shown in Fig. 1c. N_2^1 and N_1 Formations are dominated by clastic rocks. E_3^2 Formation is dominated by mixed rocks, including carbonates, gypsum rocks and mudstones. The intra-salt reservoirs (I–III) mineral composition is mainly dolomite, clay minerals, calcite, and quartz. The rock structure types include granular, porphyritic, layered, and massive structures. Dissolution pores/cavities, breccia pores/cavities, matrix pores, and a small number of faults are developed in the reservoir space, and mainly dissolution pores, intergranular pores, and breccia pores are developed in local good sections (Huang et al., 2018; Hao et al., 2020). The sub-salt reservoirs (IV–V) are mainly mud-bearing or argillaceous dolomite, and the mineral components are mainly dolomite, clay, and calcite. Compared with the intra-salt reservoirs, the contents of debris and salt rock are lower, but the anhydrite content is higher. There is development of granular, patchy, lamellar, and massive structures (Zhang et al., 2017a, b; Shi et al., 2020).

There are many types of salt minerals in the Yingxi area and they mainly include halite, gypsum or anhydrite, glauberite, and celestite (Wang et al., 2020; Liu et al., 2021). These salt minerals can be divided into two types of occurrence: salt layers of various thicknesses and salt minerals within carbonate rock in the form of mineral particles in the main reservoir section (Huang et al., 2018). The salt layers have the following vertical distribution characteristics: the salt layers of the intra-salt reservoir group are relatively well developed, and the maximum single-layer thickness can reach 5.15 m. The chemical composition is mainly rock salt (NaCl). The salt layers of the sub-salt reservoir group are thin, mostly from several centimeters to dozens of centimeters thick, and the chemical composition is mainly anhydrite ($CaSO_4$). This latter type of occurrence exists in the main reservoir section (Zhang et al., 2017a; Wang et al., 2020). The salt minerals in carbonate rocks have the following characteristics: halite is widely developed in the intra-salt reservoir group, but its distribution in the sub-salt reservoir group exhibits regional differences. Anhydrite is generally developed in the intra-salt and sub-salt reservoirs, but its content is higher in the sub-salt reservoirs. Glauberite is widely developed in the sub-salt reservoir group, and its distribution exhibits obvious regional differences. The celestite content is low (Huang et al., 2016).

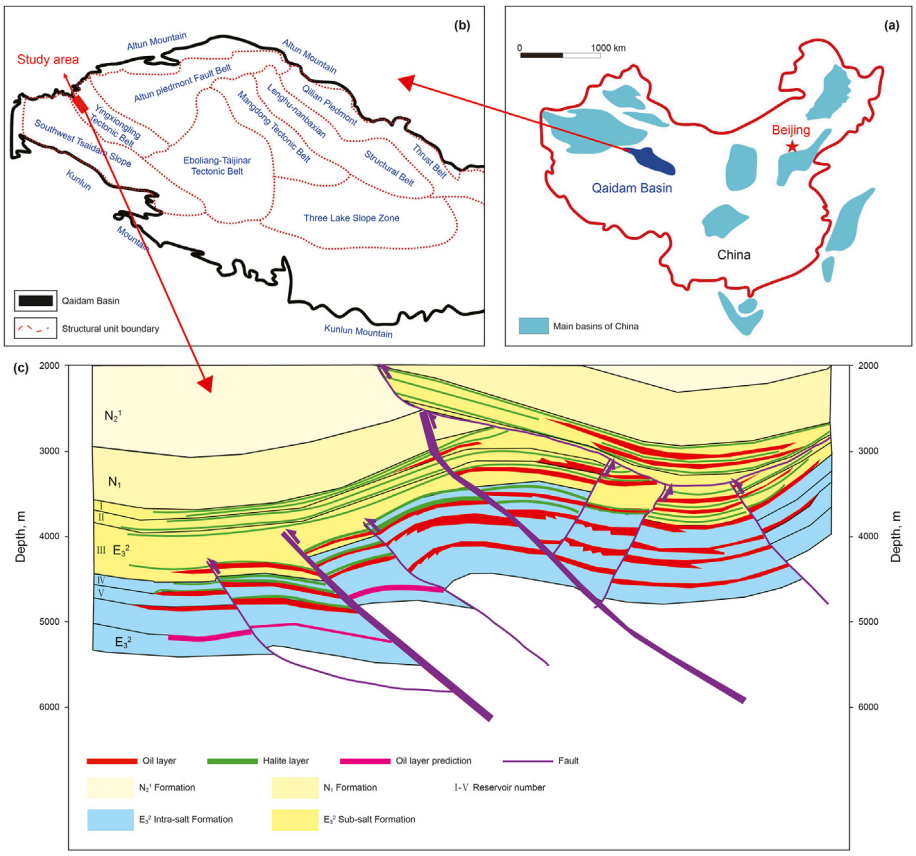

Fig. 1. Reservoir–fault profile in the Yingxi area of the Qaidam Basin.

3. Modeling tools

Reactive transport modeling is an important tool that can be used to explain lots of coupled processes (geochemical, microbial, and physical) in the earth system. TOUGHREACT numerical simulation software was utilized in this study. TOUGHREACT is coupled with a geochemical reaction module based on TOUGH. TOUGHREACT fully considers fluid–rock chemistry occurring in the reservoir diagenesis process, including equilibrium or kinetic control processes such as cation exchange, surface complexation, gas–liquid interaction, minerals dissolution/precipitation, and porosity and permeability changes. TOUGHREACT can simulate flow, heat, multicomponent solute transport, and geochemical processes during reservoir diagenesis in 1D, 2D, and 3D porous or fractured media. It can also effectively couple simulation of fluid–rock chemistry and product migration, so it can simulate rock cementation, metasomatism, dissolution, pore destruction and preservation, pore fill composition, and wettability (Xu et al., 2006).

Changes in porosity and permeability occur by mineral dissolution/precipitation. When the amount of precipitation is greater than the amount of dissolution, porosity decreases. Conversely, when the opposite occurs, porosity increases. Porosity can be calculated by the change in mineral volume fraction, as shown in Eq. (1):

$$\varphi = 1 - \sum_{m-1}^{nm} fr_m - fr_u \tag{1}$$

where nm is the mineral species, fr_m is the volume fraction of the m-th mineral, and fr_u is the volume fraction of unreacted rock.

In actual geological body, the relationship between porosity and permeability is complex, being affected by factors such as pore size, shape, distribution, and connectivity. Optional models for calculating permeability in this simulation include the following: (1) porosity is calculated based on the Carman–Kozeny relationship, ignoring particle size, curvature, and specific surface area; (2) the pore distribution, pore roar size, and pore type are calculated based on the improved Hagen–Poiseulle law; (3) a simple cubic law and the Kozeny–Carman equation of porosity and permeability are implemented, considering the geometric characteristics of the pores and the relationship between mineral precipitation location and permeability.

4. Numerical simulation

4.1. Model set up

First, a 2D profile model was established, as shown in Fig. 2. The total length in the vertical direction Z was 100 m. The top was at 0 m, the bottom was at −100 m, and the interval included the intra-salt and sub-salt reservoirs. The upper 0 to −30 m, the intra-salt reservoir, included interbedded sand and mud, which was distributed as mud–sand–mud–sand–mud layers of 6 m each, and the lower interval from −30 to −70 m was the sub-salt reservoir. The vertical direction was subdivided uniformly: each grid was 1 m, and each column included a total of 100 grids. The X direction was 35,000 m, the length was 347.13 m, and the angle was 11.63° in the range of 250–700 m. The fault was encrypted. Therefore, the X-direction had grids of 10 m × 10 m × 1 m from 0 to 1200 m, and the radial volume was increased from 1200 m to 35,000 m. The model included 14,000 grids.

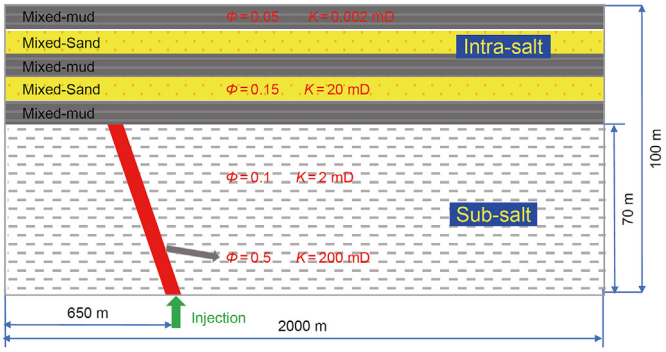

Fig. 2. Schematic diagram of numerical simulation model.

In this study, after the fluid was filled, the entire model range was not involved. The subsequent images only illustrate the fluid-involved area, that is, 0–2000 m in the lateral direction.

4.2. Simulation program

The simulation lasted 450,000 years and included two stages. The first stage was simulated for 250,000 years (0–250,000 years), aiming to study the transformation of the reservoirs caused by deep saline fluid. The simulation time of the second stage, the organic acid filling stage, was 200,000 years (250,000–450,000 years). It was used to study the subsequent transformation of the reservoir by organic acids following deep saline fluid.

4.3. Initial conditions

4.3.1. Temperature and pressure

Fig. 3 shows the relationships between pressure-altitude and temperature-depth in the Yingxi area. The reservoir between the salt is weakly over-pressured, with a pressure coefficient β of 1.2–1.6, and the reservoir beneath the salt is strongly over-pressured, with a β of 1.5–1.9. The correlation coefficient between temperature and depth is negative.

According to the depth of the model, the top temperature was set to 110 °C and the top pressure was set to 70 MPa. The pressure in each layer was calculated according to the corresponding pressure coefficient. The upper intra-salt reservoir (0 to −30 m) was weakly over-pressured, with a pressure coefficient of 1.3. The pressure at −30 m was 70.39 MPa. The interval of −30 to −100 m was strongly over-pressured. The pressure coefficient was 1.8, and the pressure at −100 m was 71.60 MPa.

4.3.2. Physical conditions

Through the long geological history of the Yingxi area, many salt layers were mixed into the sand–mud interbeds due to the attributes of the inland lakes, so the porosity is relatively complex. Porosity in the sub-salt region is mainly within 3%–11%, with an average of 6.2%. Permeability is mainly distributed within 0.02–40.2 mD, with an average of 0.61 mD. The specific distribution is shown in Fig. 2. The porosity and permeability of the subsalt reservoir were 0.1 and 2 mD, and the porosity and permeability values of fault were 0.5 and 2000 mD, respectively. The initial porosity and permeability of mud in the model were set to 0.05 and 0.002 mD, respectively. The initial porosity and permeability of sand was 0.15 and 20 mD. With the assumption that each initial formation is homogeneous, the physical parameters are shown in Table 1.

4.3.3. Hydrochemical condition

Fig. 4 shows the relationships among total organic carbon (TOC), paleosalinity, and chloride ion concentration in the study area. The paleosalinity is concentrated within a range near 20‰. Thus, the source rocks are mainly in an environment of semi-saltwater to light saltwater. According to statistics of 14 wells in the study area, the formation water density of E_3^2 in the Yingxi area is 1.1842 g/cm^3, the pH is 6.0–7.7, with an average of 6.5. The total salinity is 274,593.7 ppm and the water type are $CaCl_2$.

This model included intra-salt and sub-salt regions, with correspondingly different initial water chemical compositions. The simulation included two processes, deep saltwater upwelling and organic acid charging, respectively, so there are two external fluids. The pH value of acid is about 4.0. The cations in the solution were measured by Inductively Coupled Plasma Emission Spectrometry (ICP-AES), and the anions are determined by Ion Chromatography. The concentrations of hydrochemical ions in these models are shown in Fig. 5.

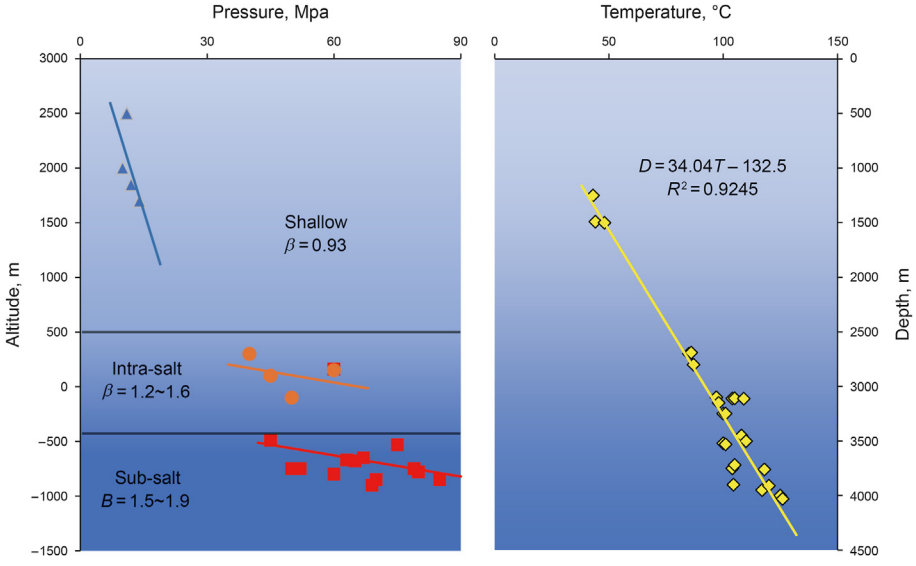

Fig. 3. Relationships between pressure and altitude and temperature and well depth.

Table 1
Parameters of physical properties used in the model.

Parameter	Mixed rock–sand	Mixed rock–mud	Sub-salt reservoir
Porosity, %	15	5	10
Horizontal permeability, mD	20	0.002	2
Vertical permeability, mD	2	0.0002	0.2
Coefficient of compressibility, Pa^{-1}	4.5×10^{-10}	4.5×10^{-10}	4.5×10^{-10}
Density of rock, kg/m^{-3}	2710	2710	2710
Thermal conductivity, W/m/°C	2.20	2.20	2.20
Specific heat of rock particles, J/kg/°C	852	852	852

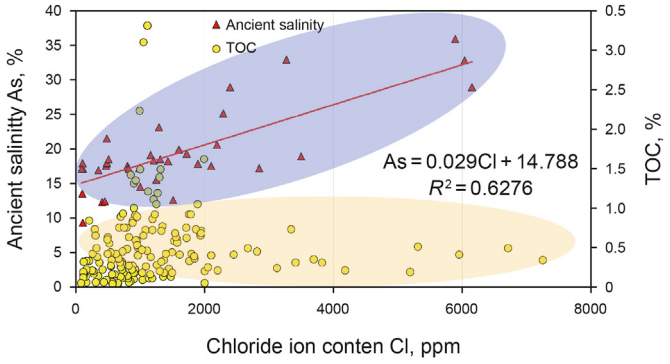

Fig. 4. Relationships among total organic carbon (TOC), paleo salinity, and chloride ion concentration.

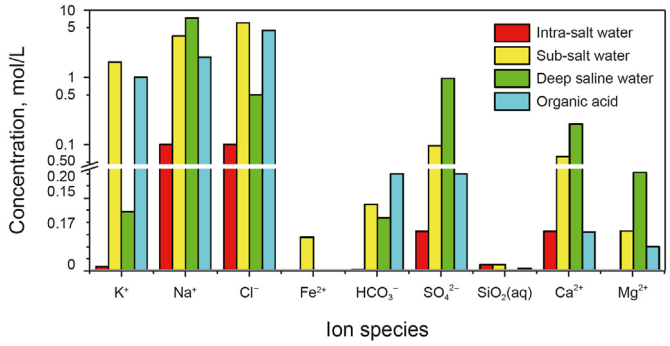

Fig. 5. Concentrations of hydrochemical ions.

4.3.4. Mineral composition and contents

Fig. 6 shows the measured mineral composition and relative contents using X-ray diffraction analysis in each layer. Among these, reservoirs I–III are intra-salt reservoirs, and reservoirs IV–V are sub-salt reservoirs. Contents of quartz, calcite, albite, and ankerite are high, and clay minerals account for 10%–50% of the total mineral content.

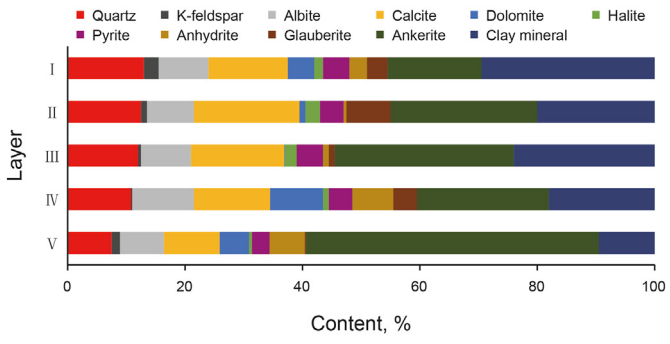

Fig. 6. Mineral composition and relative contents.

According to Fig. 6, the rock mineral composition and relative contents used in this model are shown in Table 2. The sub-salt reservoirs are dominated by carbonate minerals, feldspar, and quartz. The intra-salt mixed layer contains different amounts of rock salt and clay minerals, such as smectite and kaolinite. The mud layer contains more ankerite.

4.4. Boundary conditions

The top boundary in the model was fixed, and all physical and chemical conditions, such as pressure and ion concentration, did not change with time. The fixed boundary not only played the role of evacuation system pressure but also simulated the infinite scale of the actual formation.

Considering the structural conditions of the reservoir, the fault zone (X: 600–700 m) at the bottom of the model was injected in segments. Under different fault conditions, the velocity of hydrothermal intrusion to the seabed is 2.6–4.1 m/a (Gahtani, 2013). Therefore, during the period of 0–250,000 years, deep saline fluid was injected to the reservoir along the bottom of the faults, and the filling rate was 6.61 m/a. During 250,000–450,000 years, the injection of deep hydrothermal solution was stopped, and organic acids were filled along the bottom of the faults with a filling rate of 16.3 m/a.

5. Results

5.1. Migration of deep fluid

To analyze how the fluid flows and migrates after entering the reservoir and avoid interference from other factors such as chemical reactions, a tracer (t_skdd1) was set up in the model. The tracer did not participate in any chemical reactions. There was no tracer at the beginning of the system. The concentration of tracer in the deep hydrothermal solution was 1 mol/L, and the concentration in the organic acid influx was 2 mol/L. The flow path and concentration of tracer represented the fluid flow and diffusion.

Fig. 7 shows the concentration distribution of tracer at different times. Obviously, at time 0, the concentration of tracer in the whole model was 0 mol/L. During 0–250,000 years, with the deep hydrothermal fluid filling into the reservoir continuously, the tracer concentration increased first at the fault and then increased in the reservoir near the fault. Finally, the tracer concentration in the intra-salt reservoirs increased. This illustrates preferential fluid migration upward along the fault and then also migration to the surrounding reservoir through the upward migration process after fluid filling. Finally, some fluids break through the top of the fault and enter the intra-salt reservoir. Due to the better porosity and permeability conditions of the mixed–sand layer, the fluid migrates preferentially to the right along this layer. In 250,000 years, the tracer concentration in the fault, surroundings, and intra-salt

Table 2
Mineral composition and relative contents (wt%).

Mineral	Sub-salt reservoir	Intra-salt mixed–sand	Intra-salt mixed–mud
Calcite	25	5	25
Anhydrite	15	30	3
Quartz	20	23	12
K-feldspar	11	1.5	1
Albite	11	12	8
Dolomite	18	0	5
Halite	0	1.5	1
Ankerite	0	15	17
Na-smectite	0	3	7
Ca-smectite	0	3	7
Kaolinite	0	3	7
Illite	0	3	7

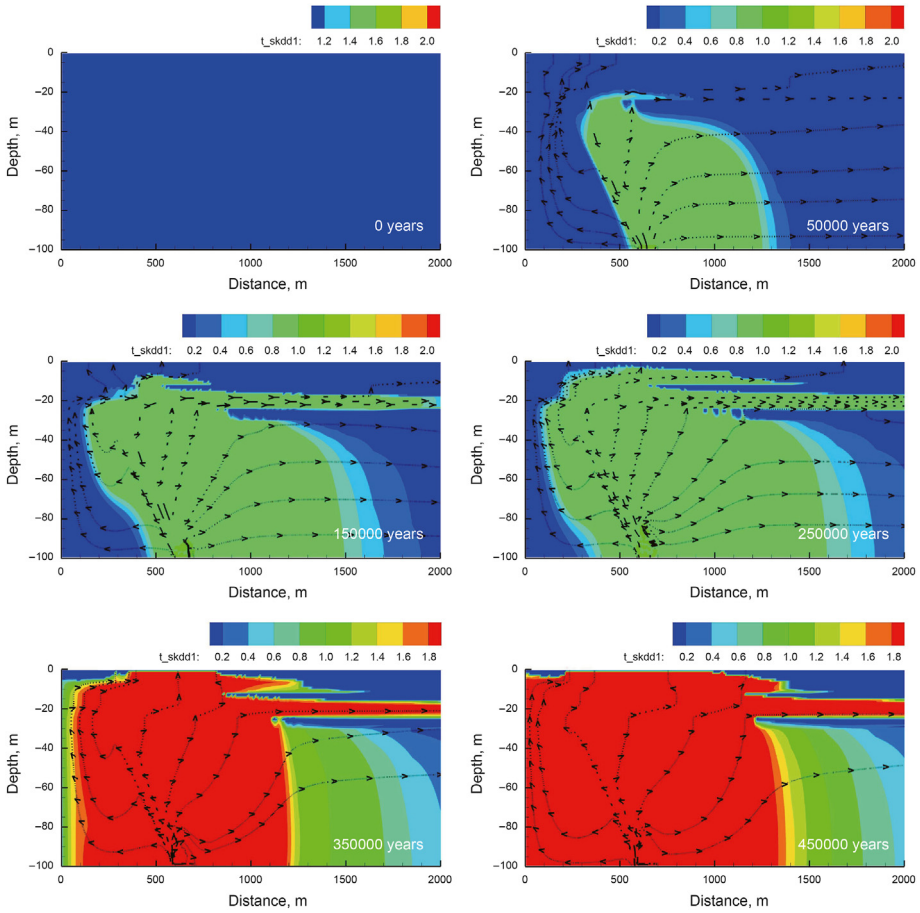

Fig. 7. Fluid flow and migration at different times.

reservoirs reached the injection concentration of 1 mol/L.

From 250,000 to 450,000 years, organic acids were filled from the bottom of the fault. Results showed that high-concentration tracer fluid still migrated preferentially along fault. The tracer concentrations of the affected reservoirs and intra-salt reservoirs around the fault, gradually increased to 2 mol/L, and the range of fluid migration continued to expand.

5.2. Transformation of reservoir minerals

Fig. 8 shows the distribution of change in the relative contents of typical minerals, such as feldspar, calcite, and anhydrite, at the end of the deep hydrothermal upwelling (250,000 years) and the organic acid filling (450,000 years).

During the deep hydrothermal upwelling (0–250,000 years), minerals dissolution and precipitation occurred mainly in the lower half of the fault in the sub-salt reservoir. Potassium feldspar and calcite dissolved, while albite, dolomite, and anhydrite precipitated. In particular, anhydrite precipitation was large, forming anhydrite veins in the lower half of the fault. In the intra-salt reservoirs, due to the wide range of fluid migration in the mixed sandstone layer, the range of mineral changes was larger than in the mud layer. However, the reaction intensity was weaker than in the mud layer. This was the case because the porosity and permeability of the mud layer are small, and fluid and surrounding minerals had more time in contact for reaction, resulting in strong chemical reaction. In the

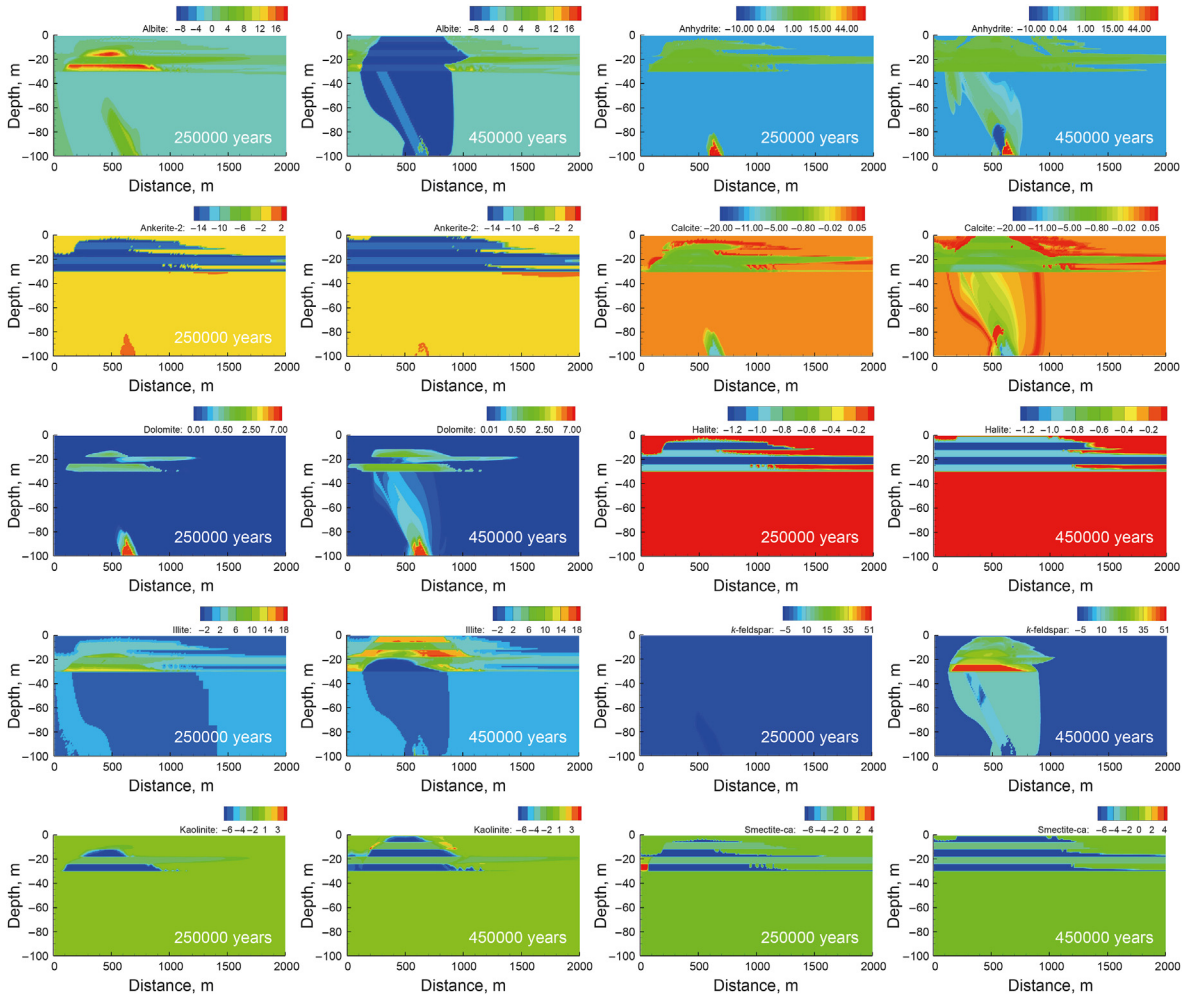

Fig. 8. Variation in typical minerals.A negative value represents a decrease in relative mineral content, i.e., mineral dissolution. A positive value represents an increase in relative mineral content, i.e., mineral precipitation.

intra-salt reservoir, salt, calcite, ankerite, kaolinite, and smectite dissolved, and albite, dolomite, anhydrite, and illite precipitated.

During the organic acid filling (250,000–450,000 years), albite continued to dissolve in the sub-salt reservoirs and precipitated slightly at the bottom of the fault. Potassium feldspar dissolved in the fault but precipitated in the surrounding reservoir. Calcite was mainly dissolved, and the dissolution range extended into the reservoir near the fault. Dolomite continued to precipitate in the fault, and a large amount of anhydrite was dissolved. The anhydrite previously precipitated in certain areas in the lower half of the fault was dissolved. In the intra-salt reservoir, salt, calcite, ankerite, and smectite were still mainly dissolved, albite, K-feldspar, dolomite, anhydrite, and illite were mainly precipitated, and the mixed–mud layer in contact with the fault showed slight dissolution.

5.3. Changes in reservoir porosity

Fig. 9 shows the distribution map of reservoir porosity at different times. The initial value set for the model at time 0 was detailed in the previous section.

During the upwelling of deep hydrothermal fluids (0–250,000 years), as fluids moved upward from faults, chemical reactions were triggered, leading to mineral dissolution or precipitation. In the sub-salt reservoir, because the total amount of precipitation of minerals was greater than the total amount of dissolution, the porosity in the fault decreased gradually, particularly in the lower part. At 250,000 years, a blockage area with a porosity close to 0.00 formed at the bottom of the fault (shown by the blue area in the Fig. 9), which was directly related to the mass precipitation of anhydrite described above.

During the organic acid filling (250,000–450,000 years), large mineral dissolution occurred as organic acids filled from the bottom of the fault. The total dissolution of minerals was greater than the total precipitation, the porosity increased gradually, and the porosity and permeability of the blocked area improved. At 350,000 years, a vertical channel with a porosity of 0.60 formed on the left side of the blocked area, resulting in a steady upward flow of organic acids. The porosity of the upper area increased gradually, as shown by the red area in the Fig. 9. The last two illustrations show the local enlarged area at the bottom of the fault, in which the vertical channel opened by organic acids is very obvious. The porosity of the intra-salt reservoir continued to increase, indicating that mineral dissolution was greater than precipitation. Because the external fluid migrated a greater distance in the mixed–sand layer, the porosity in the sand layer varied widely. However, the range of change was less than the change in the mudstone because the fluid in the mudstone had longer contact time with the surrounding minerals and thus larger amount of reaction. The initial porosity of the intra-salt mixed–sand layer was 0.15, and the initial porosity of the mud layer was 0.05. After 450,000 years of influence by external

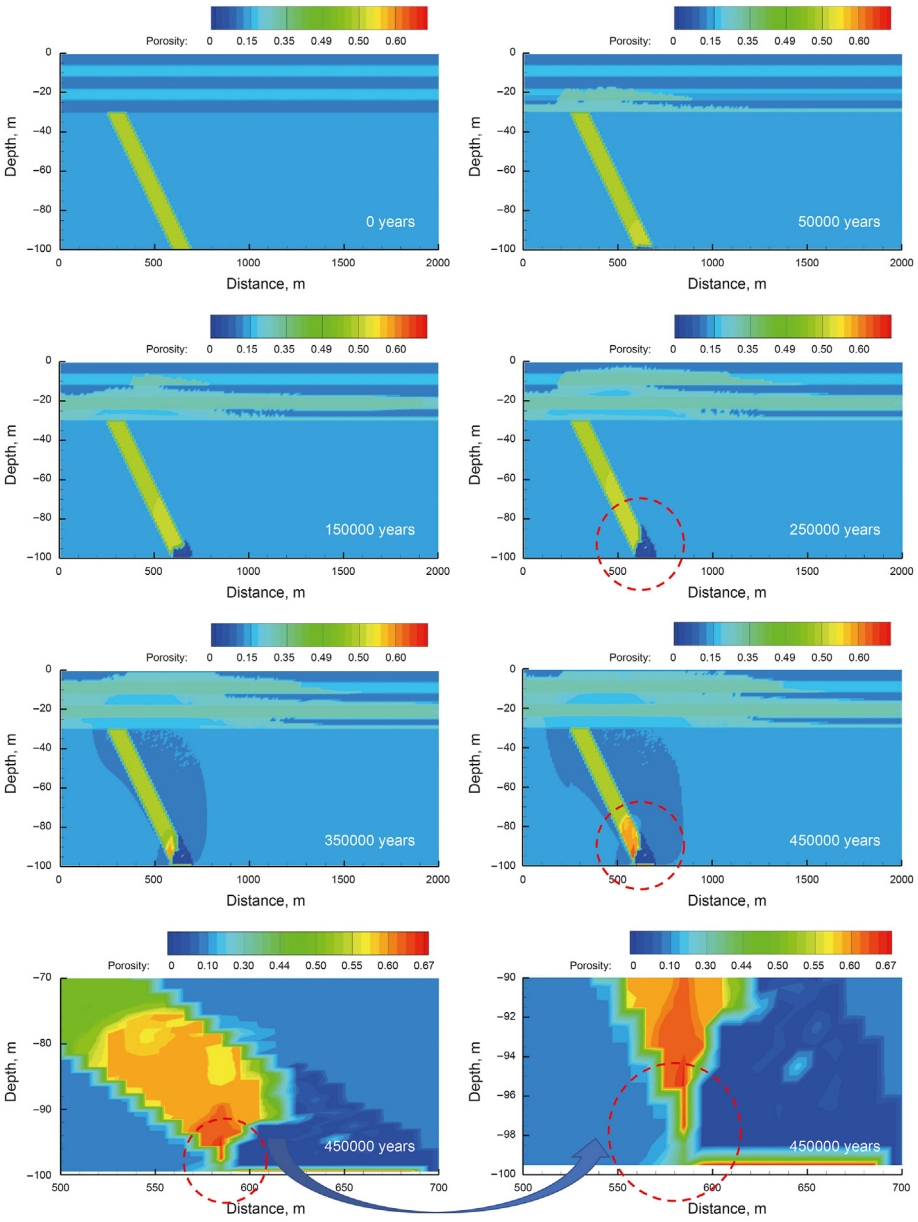

Fig. 9. Distribution maps of reservoir porosity at different times.

fluids, the porosity of mudstone had been improved greatly, and the porosity of the sand and mud layers tended to be steady at about 0.17.

6. Discussion

6.1. Alteration of the sub–salt reservoir by deep fluids

In this study, after filling by deep saline fluid, potassium feldspar and calcite dissolved and albite, dolomite, and anhydrite precipitated in the sub–salt reservoir. In particular, there was large precipitation of anhydrite, and about 50% of it precipitated in the lower half of the fault, forming an anhydrite vein. The porosity was sharply reduced to 0.0, and a blockage area formed at the bottom of the fault. The cations abundant in the saline fluid were not conducive to minerals dissolution. For example, large amounts of potassium and sodium ions inhibit the dissolution of feldspar to some extent (Crundwell, 2015). At the same time, because a large concentration of potassium ions is required in the conversion of smectite and illite–montmorillonite mixed layer clay to illite, deep saline fluid provides a large material basis for this process, which promotes the conversion of clay minerals and thus blocks pores, as shown in Eqs. (2)–(4). Therefore, most of the authigenic clay minerals in the saline lake basin deposits are illite. In addition, the effects of the saline fluid on the rock pore structure in the reservoir are obvious and generally degrading of reservoir physical properties (Kummerow and Spangenberg, 2013). Formation fluid in oil and gas fields is a complex solution containing a variety of dissolved components. This is especially the case for deep saline fluid, which contains high concentrations of ionic components. These fluids alter the original condition in the system by triggering mineral precipitation and transformation.

$$\text{Feldspar minerals} + H_2O + H^+ \rightarrow (K^+, Na^+, Ca^{2+}) + SiO_2 + Al_2Si_2O_5(OH)_4\ \text{(Kaolinite)} \quad (2)$$

$$Al_2Si_2O_5(OH)_4\ \text{(Kaolinite)} + K^+ \rightarrow KAl_3Si_3O_{10}(OH)_2\ \text{(Illite)} + H^+ + H_2O \quad (3)$$

$$\text{Smectite} + Al^{3+} + K^+ \rightarrow \text{Illite} + Na^+ + Ca^{2+} + Fe^{3+} + Mg^{2+} + Si^{4+} \quad (4)$$

Acidic fluid in a diagenetic environment is mainly related to organic acids preferentially discharged during hydrocarbon generation from source rocks. Organic acids can dissolve soluble minerals, such as calcite, in the reservoir and generate secondary pores, thereby increasing the reservoir space and permeability of the rocks (Mernagh, 2015; Safa et al., 2021). In this study, under the action of deep–origin salt fluid, anhydrite veins formed in the fault and even blocked the fault. After the organic acid filling, albite, K–feldspar, and calcite were mainly dissolved in the sub–salt reservoir, and the dissolution range extended into the reservoir near the fault. Much of the anhydrite in the fault dissolved, the porosity increased gradually, and the porosity and permeability of the blocked area improved. At 350,000 years, a vertical channel opened in the blocked area, and the porosity increased to 0.60. Organic acids migrated upward continuously, and the porosity in the upper area increased gradually to about 0.50. Obviously, the organic acids diminished the anhydrite veins in the reservoir, thus providing a channel for fluid migration and further improving the physical properties of the reservoir. The Xiaganchaigou Formation in the Qaidam Basin consists of saline lacustrine basin deposition, and gypsum is apparent in rock thin sections viewed by a polarizing microscope (Liu et al., 2021).

Acidic and alkaline diagenetic fluids jointly controlled the diagenetic environment of the reservoir, thereby affecting its development (Wang et al., 2017). Deep fluid has its controlling effect on the reservoir in two ways. Deep saline fluid leads to precipitation of salt minerals and poor reservoir properties, but organic acids promote dissolution and alleviate reservoir tightness. The formation of carbonate cements and anhydrite veins is related to alkaline fluid, and the possibility of mineral dissolution to form secondary pores that improve the reservoir is related to the activity of acidic fluid (Kazempour et al., 2013). Therefore, the activities of acidic and alkaline fluids jointly determine the development process of deep high–quality reservoirs. There are various alkaline and acid diagenetic environments in the Paleogene beach bar sandstone reservoirs in the Dongying Depression of the Bohai Bay Basin. The evolution process of the environment controls its diagenesis and storage space. There are also early dissolution of feldspar and late anhydrite cementation (Wang et al., 2017). Alkaline diagenesis often occurs in the early diagenetic process of a saline lake basin reservoir. In this process, a large amount of carbonate cements can fill the primary pores, which effectively hinders compaction and preserves primary pore space. In the Vuoriyarvi Devonian alkaline–ultramafic complex (northwest Russia), the diagenesis of deep fluids is also related to bicarbonate (Aguilera and Vargas, 2016; Prokopyev et al., 2020). In the late stage of diagenesis, the organic acid injection accompanying the polygenetic stage controls the acid diagenesis. Under acidic conditions, minerals gradually dissolve, resulting in a large number of dissolution pores. The alternation of acidic and alkaline fluids affects the development timing of large–scale secondary pores. The range of influence of the fluid is closely related to the distribution and transportation of the fault system.

6.2. Alteration of the intra–salt reservoir by deep fluids

In this study, after deep saline fluid and organic acids filling, rock salt, calcite, ankerite, and smectite were mainly dissolved in intra–salt reservoirs. Albite, dolomite, anhydrite, and illite were mainly precipitated. In the mud layer in contact with the fault, illite was slightly dissolved. The mineral dissolution of the intra–salt reservoirs was greater than the precipitation, and the porosity continued to increase. Because the external fluid travelled far in the mixed–sand layer, the contact time between the fluid and the rock was not as long as the time with the mudstone. Therefore, the variation range of porosity in the sand layer was large, but was not as large in the mud layer. The initial porosities of the sand and mud layer were 0.15 and 0.05, respectively. After 450,000 years of influence of external fluids, the porosity of the mud layer was greatly improved, and the porosity of the sand layer and mud layer tended to be consistent at about 0.17.

Different sedimentary systems or sedimentary facies belts attributable to differences in deposition, structure, and other effects, resulting in differences in reservoir porosity, permeability, minerals, solutions, biology, and more, result in reservoir heterogeneity (Bonson et al., 2007). Heterogeneity plays an important role in geological research and cannot be ignored. Many studies have shown that heterogeneities of reservoir porosity, permeability, geochemistry, and other factors have a great influence on diagenesis (Becker et al., 2017; Nader, 2017; Morad et al., 2010). The rock composition of the Sulige Gasfield is complex, mainly composed of tight sandstone and mudstone, with significant reservoir heterogeneity and poor porosity and permeability (Jia et al., 2007). Affected by these heterogeneities, the fluid–rock chemical interaction and the final content of each mineral have a strongly heterogeneous distribution in space. However, minerals are closely linked by some common ions, which exert control and influence on the minerals. Eventually, the reservoir acquires a similar heterogeneous form. For example, reactions are strong or weak in specific settings and locations, illustrating the close relationships of the common transformation of minerals. If the geological conditions of adjacent reservoirs are similar, they tend to remain consistent after the same diagenetic event.

6.3. Controlling effect of faults

In this study, during 0–250,000 years, with the deep hydrothermal fluid filling into the reservoir continuously, the tracer concentration increased first at the fault and then increased in the reservoir near the fault. Good fault conditions provide channels favorable for fluid migration. The fluid from the bottom of the reservoir quickly migrated upward. Due to the good physical conditions within the fault, a dominant channel was established, and the fluid migrated preferentially along this fault. Moreover, lateral migration produced additional reaction during this process. Therefore, the most intense reaction occurred in the fault, but there was local reaction around the fault. The faults in the Qaidam Basin are complex, and the structural belt has experienced multi–stage tectonic activities. The internal faults in the structural belt are well developed, and the structure is complex. From the previous research results, the faults exert obvious control on the structure and on oil and gas (Tondi et al., 2011; Anyim and Gan, 2020). The deep fluid is formed by seepage of surface water or shallow groundwater along the fault zone and into the deep temperature zone (Bayon et al., 2011). The heated fluid then returns to shallow levels. Previous studies have shown that salt ions entering the

gypsum–salt rocks in the Shizigou area of the Qaidam Basin are mainly injected into the lake basin by deep hot brine. For example, the tectonic movement of the XI fault provides a good channel for upwelling of deep hot brine. Fluids in Liushagang Formation in Weixinnan Depression migrate along faults, and strong dissolution occurs in major faults and secondary faults (Xie et al., 2019).

At the same time, fluid–induced chemical reactions change the permeability and structural characteristics of fault in this study. As the reaction proceeded, anhydrite veins formed at the bottom of the fault, blocking the fault and hindering fluid transport. The fault did not open again until organic acids filled the fault in the later stage of diagenesis, but the infiltration condition was still not as good as during the initial stage. Deep faults are well developed in the Qaidam Basin, and many salt lakes are located in the fault zone. The deep faults can allow oil and gas to migrate vertically. Vertical associations among multi–stage faults and lateral connections between faults and lithologies can cause oil to accumulate in favorable traps (Hillman et al., 2020; Lu et al., 2020). In the weak structural belt under the Shizigou Fault, fault activity causes salt rock flow. There is fault–dissolution pores in the deep layer of the Yingxi area, corresponding to the development of fault–cavity reservoirs controlled by faults. The Jurassic in the Tuha basin is controlled by “sweet spots” and has poor porosity and permeability (Zhou et al., 2015). Fault is the key to its reservoir characterization, and oil and gas reservoirs can be better predicted by calculating the density and strike of the fault (Moridis et al., 2010). The ways in which faults control fluid migration and reservoir reconstruction are related to the fault types and their properties.

7. Conclusions

Acidic and alkaline diagenetic fluids jointly control the diagenetic environment of the reservoir, thereby affecting its development. Formation of carbonate cements and anhydrite veins is related to the alkaline fluid. The potential of mineral dissolution to form secondary pores that improve the reservoir is related to the activity of the acidic fluid. As dominant channels, faults play a role in transporting fluid, controlling fluid migration, and controlling reservoir transformation. Therefore, the properties of the deep fluids and the distribution and transport of the fault system play decisive roles in the formation and distribution of deep, high–quality reservoirs.

Acknowledgments

This research is supported by the Natural Science Foundation of China (No. 41902045, 41702249) and the Strategic Priority Research Program of the Chinese Academy of Sciences, Grant No. XDA14010401. The English in this document has been checked by two professional editors, both native speakers of English, and they are gratefully acknowledged.

References

Acero, P., Auqué, L.F., Galve, J.P., et al., 2015. Evaluation of geochemical and hydrogeological processes by geochemical modeling in an area affected by evaporite karstification. J. Hydrol. 529, 1874–1889. https://doi.org/10.1016/j.jhydrol.2015.07.028.

Aguilera, R., Vargas, J.R., 2016. Factors controlling fluid migration and distribution in the Eagle Ford shale. SPE Reservoir Eval. Eng. 19 (3), 403–414. https://doi.org/10.2118/171626-PA.

Anyim, K., Gan, Q., 2020. Fault zone exploitation in geothermal reservoirs: production optimization, permeability evolution and induced seismicity. Adv. Geo Energy Res. 4 (1), 1–12. https://doi.org/10.26804/ager.2020.01.01.

Austad, T., Alireza, R.D., Puntervold, T., 2010. Chemical mechanism of low salinity water flooding in sandstone reservoirs. SPE Improved Oil Recovery Symposium 129767, 24–28. https://doi.org/10.2118/129767-MS.

Bayon, G., Birot, D., Ruffine, L., et al., 2011. Evidence for intense ree scavenging at cold seeps from the Niger delta margin. Earth Planet Sci. Lett. 312 (3–4), 443–452. https://doi.org/10.1016/j.epsl.2011.10.008.

Becker, I., Wüstefeld, P., Koehrer, B., et al., 2017. Heterogeneity of porosity and permeability in a tight gas sandstone reservoir analogue, Westphalian D, NW Germany: the influence of depositional setting, sedimentary architecture, and diagenesis. J. Petrol. Geol. 40, 363–389.

Belén, O.U., Agnes, K., Carsten, V., et al., 2011. Modification of the magnetic mineralogy in basalts due to fluid–rock interactions in a high–temperature geothermal system (Krafla, Iceland). Geophys. J. Int. 186 (1), 155–174. https://doi.org/10.1111/j.1365-246X.2011.05029.x.

Bonson, C.G., Childs, C., Walsh, J.J., et al., 2007. Geometric and kinematic controls on the internal structure of a large normal fault in massive limestones: the maghlaq fault, Malta. J. Struct. Geol. 29 (2), 336–354. https://doi.org/10.1016/j.jsg.2006.06.016.

Chen, D., Ren, Y., 2019. The discovery of mesoproterozoic oceanic crust in North Qaidam UHP Belt, NW China. Acta Geol. Sin. 93 (S2), 3. https://doi.org/10.1111/1755-6724.14146.

Chiaramonte, L., Zoback, M., Friedmann, J., et al., 2011. Fracture characterization and fluid flow simulation with geomechanical constraints for a CO_2–EOR and sequestration project Teapot Dome Oil Field, Wyoming, USA. Energy Proc. 4, 3973–3980. https://doi.org/10.1016/j.egypro.2011.02.337.

Covas, T.R., Rocha, Y.S., Spigolon, A.L.D., et al., 2019. Evaluation of the effects of the simulated thermal evolution of a Type–I source rock on the distribution of basic nitrogen–containing compounds. Fuel 254 (15), 115–685. https://doi.org/10.1016/j.fuel.2019.115685.

Crundwell, F.K., 2015. The mechanism of dissolution of minerals in acidic and alkaline solutions: part IV equilibrium and near-equilibrium behaviour. Hydrometallurgy 153, 46–57. https://doi.org/10.1016/j.hydromet.2014.06.009.

David, M.M., Robert, E.R., Jordon, E.B., et al., 2014. Bouse Formation in the bristol basin near amboy, California, USA. Geosphere 10 (3), 462–475. https://doi.org/10.1130/GES00934.1.

Frolov, E.N., Merkel, A.Y., Pimenov, N.V., et al., 2016. Sulfate reduction and inorganic carbon assimilation in acidic thermal springs of the Kamchatka peninsula. Microbiology 85 (4), 471–480. https://doi.org/10.1134/S0026261716040068.

Gaël, L., Bruno, C.V., Virginie, G., et al., 2018. Using salt tectonic structures as proxies to reveal post–rift crustal tectonics: the example of the Eastern Sardinian margin (Western Tyrrhenian Sea). Mar. Petrol. Geol. 96, 214–231. https://doi.org/10.1016/j.marpetgeo.2018.05.037.

Gahtani, F.A., 2013. The influence of diagenetic alterations on porosity in the triassic narrabeen group, Southern Sydney Basin, Australia. Geol. Q. 57 (4), 613–628. https://doi.org/10.7306/gq.1109.

Guo, Z.Q., Ma, Y.S., Liu, W.H., et al., 2017. Main factors controlling the formation of basement hydrocarbon reservoirs in the Qaidam Basin, western China. J. Petrol. Sci. Eng. 149, 244–255. https://doi.org/10.1016/j.petrol.2016.10.029.

Hao, B., Li, P.F., Huo, X., et al., 2020. Development characteristics and distribution control factors of oil reservoirs in southern western Qaidam Basin, China. Fresenius Environ. Bull. 29 (5), 3853–3859.

Han, J.L., Hussain, S.A., Han, F.Q., 2019. Stable chlorine isotopes in saline springs from the nangqen basin, qinghai–tibet plateau: brine genesis and evolution. J. Earth Syst. Sci. 128 (8), 206. https://doi.org/10.1007/s12040-019-1236-0.

Hélène, L., Pilar, L.S., Vanessa, E., et al., 2020. Fluid evolution of the cantung tungsten skarn, Northwest Territories, Canada: differentiation and fluid–rock interaction. Ore Geol. Rev. 127, 103866. https://doi.org/10.1016/j.oregeorev.2020.103866.

Hillman, J.I.T., Crutchley, G.J., Kroeger, K.F., 2020. Investigating the role of faults in fluid migration and gas hydrate formation along the southern hikurangi margin, New Zealand. Mar. Geophys. Res. 41 (1), 8. https://doi.org/10.1007/s11001-020-09400-2.

Huang, C.G., Yuan, X.Y., Song, C.H., et al., 2018. Characteristics, origin, and role of salt minerals in the process of hydrocarbon accumulation in the saline lacustrine basin of the Yingxi Area, Qaidam, China. Carbonates Evaporites 33 (3), 431–446. https://doi.org/10.1007/s13146-017-0350-9.

Huang, C., Zhao, F., Yuan, J., et al., 2016. The characteristics of dolomite reservoir in saline lacustrine Basin, Qaidam, China. Carbonates Evaporites 31, 307–317. https://doi.org/10.1007/s13146-015-0267-0.

Jackson, M., Hudec, M., 2017. Salt tectonics: principles and practice 2 (II), 61. https://doi.org/10.1017/9781139003988.

Jia, A., Tang, J., He, D., 2007. Geological Modeling for Sandstone Reservoirs with Low Permeability and Strong Heterogeneity in Sulige Gasfield. China Petroleum Exploration 1, 12–16+92 (in Chinese).

Jian, X., Guan, P., Fu, S., et al., 2014. Miocene sedimentary environment and climate change in the northwestern qaidam basin, northeastern Tibetan plateau: facies, biomarker and stable isotopic evidences. Palaeogeogr. Palaeoclimatol. Palaeoecol. 414 (15), 320–331. https://doi.org/10.1016/j.palaeo.2014.09.011.

Kazempour, M., Casey, C.S., Alvarado, V., 2013. Mitigation of anhydrite dissolution in alkaline floods through injection of conditioned water. Fuel 107 (9), 330–342. https://doi.org/10.1016/j.fuel.2012.10.003.

King, R.C., Morley, C.K., 2017. Wedge geometry and detachment strength in deepwater Fold–Thrust Belts. Earthence Reviews 165, 268–279. https://doi.org/10.1016/j.earscirev.2016.12.012.

Kummerow, J., Spangenberg, E., 2013. Experimental evaluation of the impact of the interactions of co2-so2, brine, and reservoir rock on petrophysical properties: a case study from the Ketzin test site, Germany. G-cubed 12 (5), Q05010. https://doi.org/10.1029/2010GC003469.

Liu, Z., Zhu, C., Li, S., et al., 2017. Geological features and exploration fields of tight oil in the cenozoic of western Qaidam Basin, NW China. Petrol. Explor. Dev. 44 (2),

217–225. https://doi.org/10.1016/S1876-3804(17)30024-1.
Liu, Z.G., Zhang, Y.S., Song, G.Y., et al., 2021. Mixed carbonate rocks lithofacies features and reservoirs controlling mechanisms in a saline lacustrine basin in Yingxi Area, Qaidam Basin, NW China. Petrol. Explor. Dev. 48 (1), 80–94.
Lu, X., Wang, Y., Yang, D., et al., 2020. Characterization of paleo–karst reservoir and faulted karst reservoir in Tahe Oilfield, Tarim Basin, China. Adv. Geo Energy Res. 4 (3), 339–348. https://doi.org/10.46690/ager.2020.03.11.
Ma, X.M., Huang, C.G., Shi, Y.J., 2019. Oil and gas enrichment patterns and major controlling factors for stable and high production of tight lacustrine carbonate rocks, A case study of Yingxi Area in Qaidam Basin, West China. Carbonates Evaporites 34 (4), 1815–1831. https://doi.org/10.1007/s13146-019-00529-9.
Mernagh, T.P., 2015. A review of fluid inclusionsin diageneticsystems. Acta Geol. Sin. 89, 697–714. https://doi.org/10.1111/1755-6724.12473.
Morad, S., Al-Ramadan, K., Ketzer, J.M., et al., 2010. The impact of diagenesis on the heterogeneity of sandstone reservoirs: a review of the role of depositional facies and sequence stratigraphy. AAPG (Am. Assoc. Pet. Geol.) Bull. 94 (8), 1267–1309. https://doi.org/10.1306/04211009178.
Moridis, G.J., Blasingame, T.A., Freeman, C.M., 2010. Analysis of Mechanisms of Flow in Fractured Tight–Gas and Shale–Gas Reservoirs. In: SPE Latin American and Caribbean Petroleum Engineering Conference. Lima, Peru. https://doi.org/10.2118/139250-MS.
Nader, F.H., 2017. Multi–scale Quantitative Diagenesis and Impacts on Heterogeneity of Carbonate Reservoir Rocks.
Németh, B., Török, K., Kovács, I., et al., 2015. Melting, fluid migration and fluid–rock interactions in the lower crust beneath the Bakony–Balaton Highland volcanic field: a silicate melt and fluid inclusion study. Mineral. Petrol. 109 (2), 217–234. https://doi.org/10.1007/s00710-015-0366-6.
Pham, T.H.V., Aagaard, P., Hellevang, H., 2012. On the potential for CO_2 mineral storage in continental flood basalts–PHREEQC batch–and 1D diffusion–reaction simulations. Geochem. Trans. 13, 5. https://doi.org/10.1186/1467-4866-13-5.
Prokopyev, I., Kozlov, E., Fomina, E., et al., 2020. Mineralogy and fluid regime of formation of the REE–late–stage hydrothermal mineralization of petyayan–vara carbonatites (Vuoriyarvi, kola region, NW Russia). Minerals 10 (5), 405. https://doi.org/10.3390/min10050405.
Rosenberg, M.J., Birgenheier, L.P., Vanden, B.M.D., 2015. Facies, Stratigraphic Architecture, and Lake Evolution of the Oil Shale Bearing Green River Formation, Eastern Uinta Basin, Utah, vol. 1. Springer Netherlands, pp. 211–249. https://doi.org/10.1007/978-94-017-9906-5-9.
Safa, K., Saeed, J., Saeid, N.A., et al., 2021. Simulation study of wormhole formation and propagation during matrix acidizing of carbonate reservoirs using a novel in-situ generated hydrochloric acid. Adv. Geo Energy Res. 5 (1), 64–74. https://doi.org/10.46690/ager.2021.01.07.
Seyyedi, M., Mahmud, H.K.B., Verrall, M., et al., 2020. Pore structure changes occur during CO_2 injection into carbonate reservoirs. Sci. Rep. 10 (1), 3624. https://doi.org/10.1038/s41598-020-60247-4.
Shi, Y.J., Xu, L., Xing, L.T., et al., 2019. Geochemical characteristics of crude oil in the continental saline lake basin: a case study of the Upper Part of the Lower Ganchaigou Formation in Yingxi, Qaidam Basin, China. Petrol. Sci. Technol. 38 (3), 232–239. https://doi.org/10.1080/10916466.2019.1694947.
Shi, Y.J., Xu, L., Huang, C., et al., 2020. The existence and significance of two kinds of effective reservoirs in deep water area of the western Qaidam Basin. Acta Geol. Sin. 94 (5), 1726–1727. https://doi.org/10.1111/1755-6724.14588.
Simpson, M.P., Bignall, G., 2016. Undeveloped high–enthalpy geothermal fields of the Taupo Volcanic Zone, New Zealand. Geothermics 59 (1), 325–346. https://doi.org/10.1016/j.geothermics.2015.08.006.
Sisavath, E., Mazuel, A., Jorry, S.J., et al., 2012. Processes controlling a volcaniclastic turbiditic system during the last climatic cycle: example of the cilaos deep–sea fan, offshore la réunion island. Sediment. Geol. 281 (12), 180–193. https://doi.org/10.1016/j.sedgeo.2012.09.010.
Tondi, E., Agosta, F., Rustichelli, A., et al., 2011. Faults and fractures in carbonates. Oil Gas J. 9 (2), 29–34.
Wang, J., Cao, Y., Song, G., et al., 2017. Diagenetic evolution and formation mechanisms of High–Quality reservoirs under multiple diagenetic environmental constraints: an example from the Paleogene Beach–Bar sandstone reservoirs in the Dongying Depression, Bohai Bay Basin. Acta Geol. Sin. 90 (1), 232–248. https://doi.org/10.1111/1755-6724.13074.
Wang, J.G., Zhang, D.W., Yang, S.Y., et al., 2020. Sedimentary characteristics and genesis of the salt lake with the upper member of the Lower Ganchaigou Formation from Yingxi Sag, Qaidam basin. Mar. Petrol. Geol. 111 (C), 135–155. https://doi.org/10.1016/j.marpetgeo.2019.08.006.
Warren, J.K., 2016. Hydrocarbons and Evaporites. Springer International Publishing.
Watanabe, N., Ishibashi, T., Noriyoshi, T., et al., 2013. Evaluation of a distribution of preferential flow paths in a fractured reservoir using GeoFlow. J. Jpn. Assoc. Pet. Technol. 78 (6), 482–490. https://doi.org/10.3720/japt.78.482.
Wilke, F.D.H., Vásquez, M., Wiersberg, T., et al., 2012. On the interaction of pure and impure supercritical CO_2 with rock forming minerals in saline aquifers: an experimental geochemical approach. Appl. Geochem. 27 (8), 1615–1622. https://doi.org/10.1016/j.apgeochem.2012.04.012.
Williams, J.D.O., Holloway, S., Williamset, G.A., 2014. Pressure constraints on the CO_2 storage capacity of the saline water–bearing parts of the bunter sandstone formation in the UK Southern North sea. Petrol. Geosci. 20 (2), 155. https://doi.org/10.1144/petgeo2013-019.
Wu, Y., Lv, J., Fang, X., et al., 2019. Analysis of favorable facies belts in reservoir of lacustrine carbonate rocks–hybrid sediments:Case study of Paleogene in Qaidam Basin. Nat. Gas Geosci. 30 (8), 1150–1157. https://doi.org/10.1176/j.issn.1672-1926.2019.05.019.
Xie, N., Cao, Y., Wang, J., et al., 2019. Diagenesis and its control on physical property of the reservoirs in the 3–(rd) member of the Paleogene Liushagang Formation in weixinan depression, beibuwan basin. Nat. Gas Geosci. 30 (12), 1743–1754.
Xu, T., Sonnenthal, E., Spycher, N., et al., 2006. TOUGHREACT–A simulation program for non–isothermal multiphase reactive geochemical transport in variably saturated geologic media: applications to geothermal injectivity and CO_2 geological sequestration. Comput. Geosci. 32 (2), 145–165. https://doi.org/10.1016/j.cageo.2005.06.014.
Yoseph, Y., Warren, W.W., 2002. Hydrogeologic processes in saline systems: playas, sabkhas, and saline lakes. Earth Sci. Rev. 58 (3), 343–365. https://doi.org/10.1016/S0012-8252(02)00067-3.
Zhang, H., Chen, G., Zhu, Y., et al., 2017a. Discovery and significance of dolomites altered by hydrothermal fluid in Oligocene reservoirs of the Yingxi area, Qaidam Basin. Geol. Sci. Technol. Inf. 36 (1), 87–97.
Zhang, J., Zhang, J., Yang, Q., et al., 2016. Characteristics and genesis of gypsum–salt rocks in western Qaidam Basin. J. NW Univ. 46, 866–876, 06.
Zhang, L., Chen, R., Zheng, Y., et al., 2017b. Whole–rock and zircon geochemical distinction between oceanic–and continental–type eclogites in the North Qaidam orogen, Northern Tibet. Gondwana Res. 44, 67–88. https://doi.org/10.1016/j.gr.2016.10.021.
Zhou, L., Yuan, J., Ren, D., et al., 2015. Forecast on the advantageous area distribution of tight sandstone sweet spots reservoir in Sangonghe Formation Wenjisang Area of Turpan–Hami Basin. Nat. Gas Geosci. 26 (6), 1003–1015. https://doi.org/10.11764/j.issn.1672-1926.2015.06.1003.
Zou, C., Zhu, R., Chen, Z., et al., 2019. Organic–matter–rich shales of China. Earth Sci. Rev. 189, 51–78. https://doi.org/10.1016/j.earscirev.2018.12.002.